Effect of Al presence and synthesis method on phase composition of the hydrogen absorbing La–Mg–Ni-based compounds

Matylda N. Guzik[1,], Julien Lang[2], Jacques Huot[3], Sabrina Sartori[4]*

[1]Department of Physics, University of Oslo, Blindern, P.O. Box 1048, 0316 Oslo, Norway

[2]Canadian Nuclear Laboratories, Chalk River, Ontario, Canada K0J 1J0

[3]Université du Québec à Trois-Rivières, 3351 des Forges, Trois-Rivières, Québec, Canada G9A 5H7

[4]Department of Technology Systems, Section for Energy Systems, University of Oslo, P.O. Box 70, 2027 Kjeller, Norway

[*]Corresponding author, e-mail address: m.n.guzik@smn.uio.no, postal address: Oslo Science Park, Gaustadalléen 21, N-0349 Oslo, Norway

Abstract

Results for $(La.Mg)Ni_{3.5}$ and $(La.Mg)(Ni,Al)_{3.5}$ systems synthesized by metallurgical and mechanochemical techniques are reported. Powder X-ray and neutron diffraction combined with Rietveld refinements and profile analysis show that depending on the applied synthesis method various structurally related phases can be obtained for the same nominal composition. The hexagonal A_2B_7-type structure incorporating aluminum, with the refined composition ~~of~~ $La_{0.77}Mg_{0.23}Ni_{3.41}Al_{0.09}$, has been identified. Al atoms occupy 12 % of the *6h* site within the $LaNi_5$ slabs. This intermetallic phase absorbs hydrogen (deuterium) when exposed to 10 bar of H_2 (D_2) gas at room temperature. The H(D)-containing phase expands isotropically and retains the original symmetry of the parent compound.

Keywords: Hydrogen storage materials, mechanical alloying, A_2B_7-type structure, superlattice compounds, powder X-ray diffraction, powder neutron diffraction

1. Introduction

A_2B_7-type intermetallics, crystallizing with hexagonal, *P6₃/mmc,* or rhombohedral, *R-3m*, symmetry, are examples of superlattice compounds, which have gained lots of interest during the last two decades due to their application as a negative electrode in nickel-metal hydride (Ni-MH) batteries [1-4]. Particular attention has been given to A_2B_7-type compounds in the La–Mg–Ni system, which are reported to have 25 % higher discharge capacity than any of AB_5-based materials [5-11]. $(La,Mg)_2Ni_7$ compositions reveal a superior cycle life and an overall electrochemical performance as compared to conventionally used alloys [12]. Due to these characteristics $(La,Mg)_2Ni_7$ phases are holding a strong position in the HEV automotive industry and becoming a competitive force in both, consumer and industrial Ni-MH battery markets (e. g. FDK Inc. produces long cycle-life consumer batteries (over 6000 cycles) and Kawasaki Heavy Industries builds large capacity, high power stationary batteries for industrial applications) [1, 13, 14]. Since their introduction by Sanyo (Eneloop) in 2005, A_2B_7-type compounds have been extensively investigated and developed [1, 10, 15-18]. The main research has focused on alloying of La–Mg–Ni-based phases with other elements (on the A and B site) that could extend the cycle life even further and eliminate the poor response of the compounds to the corrosion. One of the elements claimed to successfully enhance the performance of this material group is aluminum [5, 19-23]. Though electrochemical performances of substituted $(La,Mg)_2(Ni,Al)_7$ alloys have been already studied, still little is known about the structural properties of modified phases and the Al influence on the hydrogen storage capacity and thermal stability [20, 24, 25]. One of the main obstacles delaying research and development in this area is the difficulty in preparation of single phase samples [21, 26]. Most data refer to powder mixtures of structurally related superlattice

compounds, e. g. AB_3, A_2B_7, A_5B_{19} [1, 4, 26-29]. It is believed that a synergetic effect, resulting from a random coexistence of these highly hydrogen absorbing intermetallics, influences the sorption properties of such a blend, rather than structural changes induced in the A_2B_7 compounds alone. In order to gain better understanding of structural factors correlated with Al presence, reduction or complete removal of additional phases from studied samples is essential. This has been successfully demonstrated in our previous study on the La–Mg–Ni system through the synthesis of single phase samples [30].

Preparation of superlattice compounds is commonly performed by conventional metallurgical methods based on induction/arc melting and sintering [31]. However, recently, nonequilibrium techniques (e.g. spark plasma sintering, melt spinning) have also been applied [32, 33]. Ball milling was reported to ~~enable~~ facilitate formation of compounds with A_2B_7- and AB_3-type structures [22, 34]. This ~~is a~~ well-recognized technique, used for synthesis of a great variety of compositions for energy conversion and storage,~~. It~~ enables cheap and fast production of materials in a high yield ~~having also the advantage of being a fast and low cost method~~ [33]. If successfully applied for formation of intermetallics commercially used in Ni-MH batteries, it could become an interesting alternative for the currently used technologies.

The present study focuses on the comparative structural analysis of the ~~A_2B_7-type~~ superlattice compounds and their hydrides/deuterides in the Al-substituted La–Mg–Ni system, in view of applied synthesis methods with a different degree of versatility.

2. Materials and methods

2.1 Synthesis of intermetallics and their deuterides

All intermetallics were synthesized from high purity elements (> 99.9 %, La, Mg, Ni, Al) by arc/induction melting (AM/IM) and ball milling (BM), applied separately or jointly (Table 1). Two series of compounds were fabricated, one in the La–Mg–Ni system and one in La–

Mg–Ni–Al system. Two samples of $La_{0.774}Mg_{0.258}Ni_{3.268}$ were prepared (hereafter referred to as: A_{BM} and $A_{AM/BM}$). For A_{BM}, the elemental powder mixture of Mg, Ni and La was milled using a planetary ball mill (Fritsch P7) at a rotational velocity of 200 rpm, for 8 hours and under Ar atmosphere (ball to powder mass ratio (BTP) = 6). $A_{AM/BM}$ sample was obtained by mechanochemical processing of a melted and grinded La-Ni precursor ingot with a stoichiometric amount of Mg powder. Milling was carried out in the same way as for A_{BM} but just for 4 hours. The La–Mg–Ni–Al-based~~containing~~ samples were prepared according to the following nominal compositions: $La_{0.774}Mg_{0.258}Ni_{3.198}Al_{0.07}$ ($B_{AM/BM}$-$Al_{0.07}$), $La_{0.774}Mg_{0.258}Ni_{3.168}Al_{0.1}$ (B_{AM}-$Al_{0.1}$), $La_{0.774}Mg_{0.258}Ni_{3.068}Al_{0.2}$ ($B_{AM/IM}$-$Al_{0.2}$), $La_{0.774}Mg_{0.258}Ni_{3.018}Al_{0.25}$ (B_{AM}-$Al_{0.25}$). $B_{AM/BM}$-$Al_{0.07}$ was the only composition for which mechanochemical processing was applied as part of the synthesis route. The powder was prepared in the same way as $A_{AM/BM}$ and Al/Mg powder mixture was added before ball milling. For the remaining compositions either arc or induction melting was applied. Bedsides Al concentration, the other parameter varied during synthesis was an initial form of raw elements/materials (Table 1). B_{AM}-$Al_{0.1}$ was obtained according to the procedure described in [30] and Mg and Al were added as a powder mixture before annealing. The $B_{AM/IM}$-$Al_{0.2}$ series was prepared in three batches and each of them in a different way. While ~~the~~ first batch (B_{IMPC}-$Al_{0.2}$) was obtained by induction melting of element pieces (IMPC) under argon atmosphere, the second one (B_{IMP}-$Al_{0.2}$) was fabricated by induction melting of a pressed pellet (IMP) of an elemental powder mixture. The last batch (B_{AM}-$Al_{0.2}$) was obtained by ~~simple~~ convetional arc melting. The last of studied compositions (B_{AM}-$Al_{0.25}$) was prepared in an arc furnace as described earlier. Regardless of the applied methodology, obtained powders were subsequently grinded, cold pressed in a pellet and sealed under argon atmosphere (1 bar) in stainless steel tubes to eventually be heat treated. The applied scheme included annealing at 1223 K for 4 days, in a protective oxygen-free atmosphere, followed by

water quenching. Selected samples were hydrogenated/deuterated either *ex situ*, in a stainless steel autoclave, or *in situ*, in a vanadium holder during powder neutron diffraction experiments. In both cases the same hydrogenation/deuteration conditions were applied. Powder samples were first evacuated under dynamic vacuum at 350-400 °C, cooled down to room temperature and then loaded with H_2/D_2 gas in a pressure range of 5–20 bars. For selected compositions, amount of absorbed deuterium was calculated from the volumetric difference using the Peisl's relationship [35].

Table 1. Nominal compositions and synthesis details for investigated samples in the La-Mg-Ni and La-Mg-Ni-Al systems.

sample	nominal composition	synthesis method	form of raw materials	synthesis details
A_{BM}	$La_{0.774}Mg_{0.258}Ni_{3.268}$	ball milling	powder	8 h, 200 rpm, BTP = 6
$A_{AM/BM}$	$La_{0.774}Mg_{0.258}Ni_{3.268}$	arc melting/ball milling	AM: pieces BM: powder	AM: La+Ni BM: La-Ni + Mg 4 h, 200 rpm, BTP = 6
$B_{AM/BM}$-$Al_{0.07}$	$La_{0.774}Mg_{0.258}Ni_{3.198}Al_{0.07}$	arc melting/ball milling	AM: pieces BM: powder	AM: La+Ni, BM: La-Ni + Mg/Al 8 h, 200 rpm, BTP = 6
B_{AM}-$Al_{0.1}$	$La_{0.774}Mg_{0.258}Ni_{3.168}Al_{0.1}$	arc melting	pieces + powder	AM: La+Ni SSR: La-Ni + Mg/Al
$B_{AM/IM}$-$Al_{0.2}$/series				
B_{IMPC}-$Al_{0.2}$	$La_{0.774}Mg_{0.258}Ni_{3.068}Al_{0.2}$	induction melting	pieces	La+Mg+Ni+Al
B_{IMP}-$Al_{0.2}$	$La_{0.774}Mg_{0.258}Ni_{3.068}Al_{0.2}$	induction melting	powder	La+Mg+Ni+Al
B_{AM}-$Al_{0.2}$	$La_{0.774}Mg_{0.258}Ni_{3.068}Al_{0.2}$	arc melting	pieces + powder	AM: La+Ni SSR: La-Ni + Mg/Al
B_{AM}-$Al_{0.25}$	$La_{0.774}Mg_{0.258}Ni_{3.018}Al_{0.25}$	arc melting	pieces + powder	AM: La+Ni SSR: La-Ni + Mg/Al

2.2 Powder X-ray and Neutron Diffraction (PXD &PND)

Laboratory powder X-ray diffraction (PXD) data were collected with a monochromator-equipped Bruker D8 diffractometer ($\lambda = Cu_{K\alpha 1}$, step-size: 0.02° 2θ, Bragg-Brentano geometry). Neutron powder diffraction experiments were carried out only for selected compositions, at the Canadian Nuclear Laboratories (Chalk River, Canada). Samples were measured in an airtight vanadium cylindrical sample holder with the high-resolution 800 wire DUALSPEC C2 neutron powder diffractometer (λ = 1. 1.3285 Å, step-size: 0.1° 2θ). The structural analyses (La Bail profile analysis and Rietveld refinement) were performed with FullProf Suite [36]. X-ray scattering factors and neutron cross-sections were taken from the software library. Backgrounds of PXD data were defined by extrapolations between manually chosen points, while for PXD data were refined with Chebyshev polynomial. The diffraction profiles were modeled using Pseudo-Voigt or Thompson-Cox-Hasting pseudo-Voigt function.

3. Results and discussion

3.1 La-Mg-Ni and La-Mg-Ni-D systems

PXD data collected for annealed $A_{AM/BM}$ and A_{BM} confirm presence of multiple crystalline phases in both samples. Diffraction peaks in the $A_{AM/BM}$ ~~diffraction~~ powder pattern (Figure 1A) are successfully assigned to the hexagonal A_2B_7-type structure except for one intense reflection at 32.19° 2θ, which can be indexed with the rhombohedral A_2B_7 phase (2:7*R*) ~~structure~~. The lattice constants calculated for the hexagonal phase are in agreement with previously published values for $La_{0.82}Mg_{0.18}Ni_{3.5}$ [30], (*a* = 5.04871(9) vs. 5.04731(8) Å, *c* = 24.3472(6) vs. 24.3186(4) Å and *V* = 537.45(2) vs. 536.52(2) $Å^3$) but are bigger than ~~from~~ the unit cell parameters reported for $La_{0.75}Mg_{0.25}Ni_{3.5}$ [37] (*a* = ~~5.~~5.0285(2) Å, *c* = 24.222(2) Å, *V* = 530.42(4) $Å^3$, both reference samples prepared by arc melting/annealing).

The refined composition of 2:7*H* is $La_{0.83}Mg_{0.17}Ni_{3.5}$ and its abundance in the sample accounts for and 82(2) wt.% (Table 2).

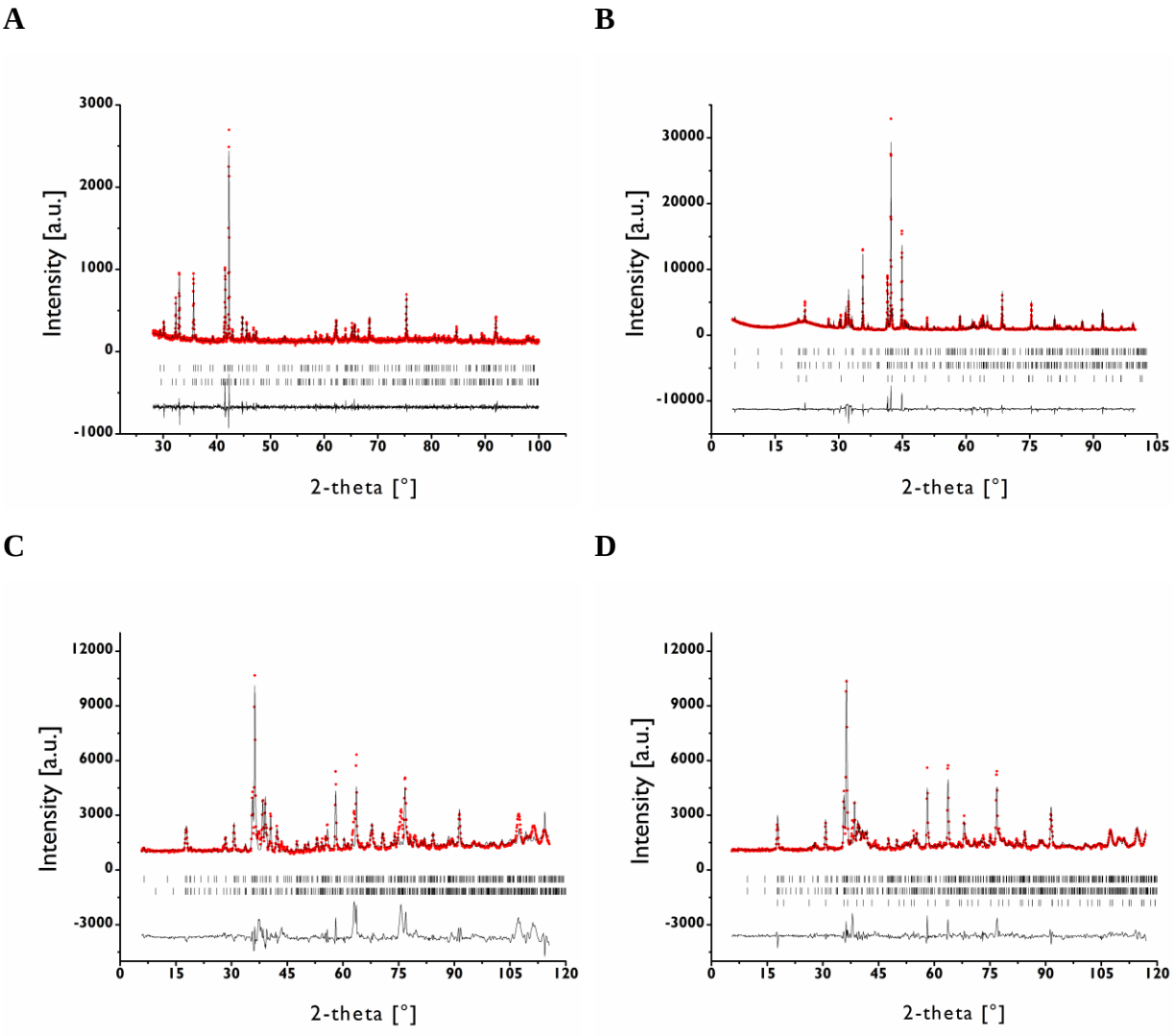

Figure 1. Observed (red), calculated (black) and difference (bottom) PXD (**A**, **B**: λ = 1.54056 Å) and PND (**C**, **D**: λ = 1.32845 Å) profiles obtained for $\mathbf{A_{AM/BM}}$ (**A**, **C**) and $\mathbf{A_{BM}}$ (**B**, **D**) samples. Vertical bars indicate the Bragg peak positions of contributing phases (from top to bottom: **A**: 5:19*R*, 5:19*H* and 1:5*H*, χ^2 = 6.0; **B**: 2:7*H*, 2:7*R*, χ^2 = 2.3; **C**: 5:19*R*, 5:19*H* and 1:5*H*, χ^2 = 7.2; **D**: 2:7*H*, 2:7*R*, χ^2 = 22.0).

For 2:7*R*, the refined lattice constant a = ~~(~~5.0432(4) Å~~)~~ is larger ~~bigger~~ than values previously obtained for $La_{0.68}Mg_{0.32}Ni_{3.5}$ [38] and $La_{0.76}Mg_{0.24}Ni_{3.5}$ [39] (a = 5.035 and 5.0328(3) Å; c = 36.309 and 36.249(9) Å, reference samples synthesized by arc melting/annealing and spark plasma sintering, respectively), while c ~~parameter (~~ = 35.969(3) Å appears smaller from the reported numbers. The calculated unit cell volume is also contracted as compared with isostructural ternary phases (V = 792.2(1) vs. 797.1 and 795.3 $Å^3$, respectively). The refined composition of the rhombohedral phase and its abundance in the sample is $La_{0.68}Mg_{0.32}Ni_{3.5}$ and 18(2) wt.%, respectively. Interestingly, even though the refined amount of magnesium in this structure is the same as ~~in the composition~~ reported for $La_{0.68}Mg_{0.32}Ni_{3.5}$ [38], magnesium atoms occupy only one of two available *6c* sites, as in $La_{0.76}Mg_{0.24}Ni_{3.5}$ [39], which has a lower Mg content. PXD data of A_{BM} (Figure 1B) suggest formation of three crystalline phases in the sample, two polymorphs of A_5B_{19} (hexagonal 5:19*H* (43 wt.%), rhombohedral 5:19*R* (50 wt.%)) and $LaNi_5$ (7 wt.%, hereafter referred to as 1:5*H*). The unit cell volume of the hexagonal 5:19*H* phase is reduced as compared to the isostructural binary La_5Ni_{19} (V = 712.16(5) vs. 720.6 $Å^3$, reference sample synthesized by induction melting/annealing) [40], but both rhombohedral and hexagonal cells are larger from previously reported values for Mg-containing ternary compositions (V = 712.16(5) vs. 702.8 and 704.7(2) $Å^3$ for 5:19*H*, and V = 1067.60(7) vs. 1054.8 and 1058.69(9) $Å^3$ for 5:19*R*; reference samples obtained by induction melting/annealing and spark plasma sintering, respectively) [39-41]. This may indicate lower magnesium concentration in both structures as compared to the reported La_4MgNi_{19} phases [39-41]. The refined compositions of the La–Mg–Ni-based phases in A_{BM} account for $La_{0.88}Mg_{0.12}Ni_{3.8}$ and $La_{0.87}Mg_{0.13}Ni_{3.8}$ for 5:19*R* and 5:19*H*, respectively (Table 2).

Table 2. Unit cell parameters and phase abundance of intermetallic compounds and their deuterates in the La-Mg-Ni system as obtained from the analysis of PXD data.

sample	**phase & space group**	***intermetallic compounds***				***deuterides***			
		a [Å]	*c* [Å]	*V* [Å^3]	phase abundance [wt.%]	*a* [Å]	*c* [Å]	*V* [Å^3]	*ΔV/V* [%]
A_{BM}	5:19*R* (*R-3m*)	5.0416(2)	48.500(2)	1067.60(7)	50(1)	5.3991(7)	50.01(1)	1262.5(4)	18.3
	5:19*H* (*$P6_3/mmc$*)	5.0422(2)	32.345(1)	712.16(5)	43(1)	5.410(1)	32.991(9)	836.3(3)	17.4
	1:5*H* (*P6/mmm*)	5.0257(-)	3.983(-)	87.13(-)	7.0(4)	5.399(2)	4.299(2)	108.56(8)	24.6
$A_{AM/BM}$	2:7*H* (*$P6_3/mmc$*)	5.04871(9)	24.3472(6)	537.45(2)	82(2)	5.3658(6)	26.490(4)	660.5(1)	22.9
	2:7*R* (*R-3m*)	5.0428(4)	35.972(3)	792.2(1)	18(2)	5.3171(4)	37.543(3)	919.2(1)	16.3

None of the prepared powders forms a single phase sample, even though previously, the same nominal composition crystallized as a single $La_{0.82}Mg_{0.12}Ni_{3.5}$ phase [30]. In addition, phase compositions of two nominally identical samples, obtained by different synthesis methods, also vary. It has been shown that 2:7*H/R* and 5:19*H/R* superlattice structures in the La–Mg–Ni system occur in a very narrow temperature range [39, 42-44] and different temperatures are reported for formation of stable A_2B_7 and A_5B_{19} phases [42, 44]. Recent data also suggest that the thermodynamic processes responsible for a phase occurrence in the ternary La–Mg–Ni system do not depend exclusively on annealing/sintering temperatures but are additionally altered by the composition and abundance of phases present in the as-cast samples [42-44]. Our study~~ies~~ clearly shows that an applied synthesis method~~ology~~ and a form of raw elements/~~materials~~precursors can also influence the abundance and chemical composition of ~~formed~~crystallizing phases. Additionally, ~~they~~it confirms that a sample phase composition can be drastically changed by a modification of Mg content [39, 44, 45]. Upon mechanical milling, which was applied for the synthesis of ~~both~~ presented ternary compositions, small amount of powder covers milling media (balls and the vials) and is irretrievably lost during sample processing. This easily disregarded powder quantity appears indispensable for formation of 2:7*H/R* and 5:19*H/R* superlattice compounds, which are highly composition-sensitive phases. Our results suggest that the decreasing Mg concentration, due to prolonged mechanochemical processing, stabilizes formation of A_5B_{19}-rather than A_2B_7-type structures, which is in keeping with recently reported work for the ternary La–Mg–Ni system [16, 39, 40, 42].

The obtained results clearly demonstrate ~~show~~ that the methods used for the synthesis of La–Mg–Ni-based superlattice compounds, and involving mechanochemical sample processing, require extended optimization to provide reproducible results. In order to form desired superlattice crystal structures, they need be ~~used~~ applied very carefully, what

questions their long-term benefit as compared with the reliable and commonly used metallurgical techniques.

The PND patterns collected for hydrogen/deuterium free intermetallics (Figure 1C and 1D) were refined against the same crystal structure models, which were used for the PXD data analysis. While for A_{BM} the calculated structural parameters are similar to those obtained from the PXD data refinements (Figure 1D), for $A_{AM/BM}$ PND pattern reveals two high-angle diffraction peaks of a secondary phase, which cannot be fitted with the rhombohedral A_2B_7-type structure alone, as the X-ray diffraction pattern (Figure 1C). Various pure elements, binary/ternary compositions and oxides were used to index missing reflections but none of the applied models improved the agreement between the observed and calculated diffraction data. This example of incomplete phase identification appears however interesting in view of all studies pursued on superlattice alloys in the multiphase samples. It shows that in systems prone to formation of closely correlated crystal structures, the analysis of just a single set of PXD data is not always sufficient to correctly identify crystalline phases present in a sample and can lead to misinterpretations of results. While scattering contrast provided by neutrons is widely used for structural studies of hydrogenated/deuterated systems, PND experiments performed on hydrogen/deuterium-free absorbing alloys are not very common. Our results demonstrates the benefit of using PND for investigation of structurally similar phases, as in the presented multiphase samples of the La-Mg-Ni system, in order to verify an accuracy of results obtained by PXD. The idea has been recently explored and complemented by time and temperature resolved neutron diffraction studies of the La–Mg–Ni-based battery alloys [43].

The A_{BM} and $A_{AM/BM}$ samples were deuterated *in situ*. In both deuterium absorption occurred almost immediately, what was associated with a strong exothermic effect reflected in a sharp increase of the sample temperatures. In PND patterns ~~collected for~~ of the deuterated A_{BM} a shift of all diffraction peaks towards lower 2θ angles upon exposure to

deuterium gas is observed (Figure 2B). This indicates that all phases present in the sample ~~powder~~ are deuterium-active under the applied conditions. Neither obvious formation nor splitting of Bragg peaks is observed, suggesting that D-absorbing phases retain their original symmetry. The largest increase of a unit cell volume is observed for 1:5*H* ($\Delta V/V$ = 24.6 %), while 5:19*H* and 5:19*R* structures expand by 17.4 % and 18.3 %, respectively (Table 2). The refined lattice constants (*a* = 5.399(2) Å, *c* = 4.299(2) Å) for the deuterated 1:5*H* phase are enlarged as compared to values reported in [44, 46] and similar to data obtained in [41]. For the deuterium containing 5:19*H*, the refined unit cell parameters are: *a* = 5.410(6), *c* = 32.991(9) Å. The *a* parameter is similar to those reported in [46] (*a* = 5.402(1) Å) and [41] (*a* = 5.4000(8) Å), while *c* parameter is somewhat smaller when compared to the previously studied compositions (*c* = 34.73(1) Å and 34.879(3) Å, respectively) [41, 46]. The unit cell of deuterated 5:19*R* reveals the same tendency. An expansion ~~in~~ of the basal *ab* plane (*a* = 5.3991(7) Å) ~~can be compared~~ is comparable with changes observed for the isostructural phases presented in [46] (*a* = 5.405(1) Å) and in [41] (*a* = 5.3990(3) Å), but its elongation in the *c* axis direction is significantly smaller (*c* = 50.01(1) Å vs. 52.33(1) and 53.990(3) Å, respectively) [41, 46]. The observed deuterium absorption is associated with substantial peaks broadening and increased diffuse scattering contribution. This could point to formation of modified microstructures, fractional phase amorphisation/segregation and/or deuterium-induce partial loss of structural long-range ordering. The PND data for $A_{AM/BM}$ were collected for the as-synthesized, absorbed and desorbed powders (Figure 2A). Upon deuteration the Bragg peaks of the hexagonal and rhombohedral A_2B_7 phases moved towards lower 2θ angles indicating the expansion of the unit cells without symmetry modification, which is in keeping with previously reported studies [30, 37]. The calculated values of lattice constants for deuterated 2:7*H* are: *a* = 5.3658(6) Å, *c* = 26.490(4) Å, and the expansion of the unit cell volume is 22.9 %. The observed volume change is smaller than for $La_{1.5}Mg_{0.5}Ni_7D_{8.9}$ [37]

($\Delta V/V$ = 25.2 %) and $La_{1.63}Mg_{0.37}Ni_7D_{8.8}$ [30] ($\Delta V/V$ = 25.6 %). For the deuterated 2:7*R*, the refined unit cell parameters are: *a* = 5.3171(4) Å, *c* = 37.543(3) Å and the unit cell volume expands by 16.3 %. Obtained values are smaller from those reported in [41] (*a* = 5.3968(8) Å, *c* = 39.383(7) Å) and in [46] (*a* = 5.377(2) Å, *c* = 38.36(2) Å) for the same crystal structures. The D-containing $A_{AM/BM}$ sample, when exposed to the ambient argon pressure, desorbed deuterium completely. The process is confirmed by a visible shift of the corresponding Bragg peaks to the same position, as observed for the intermetallic phases in the as-synthesized sample (Figure 2A). Interestingly, two unidentified peaks in the PND data do not change position during deuterium absorption/desorption process. This indicates that the phase either does not store hydrogen/deuterium or requires different pressure and temperature conditions for the absorption to occur.

A **B**

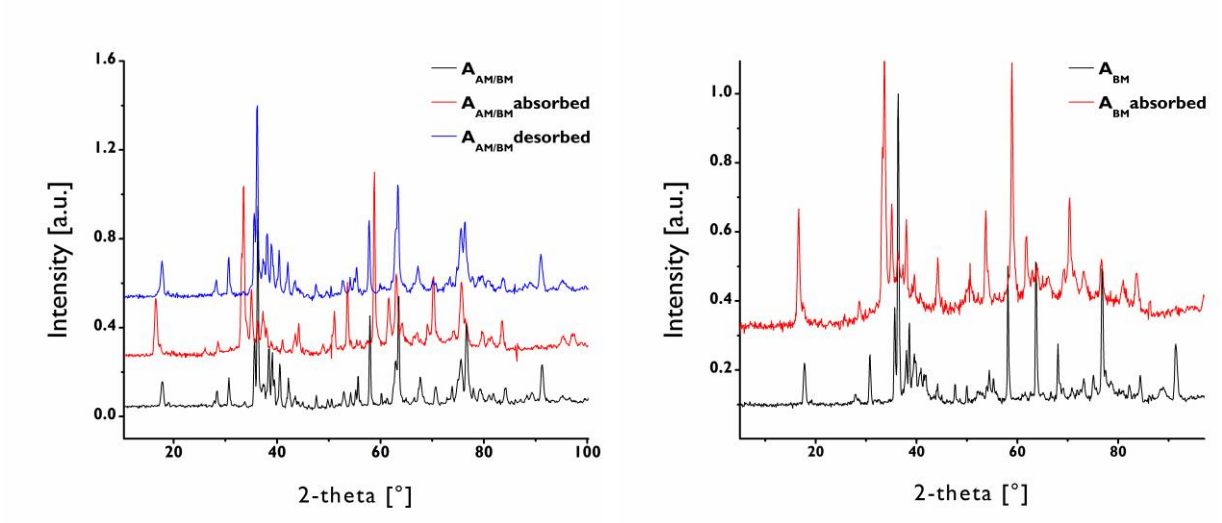

Figure 2. PND patterns (λ = 1.32845 Å) collected for the annealed (black), D-absorbed (red) and D-desorbed (blue) $\mathbf{A_{AM/BM}}$ sample (**A**) and the annealed (black) and D-absorbed (red) $\mathbf{A_{BM}}$ sample (**B**).

3.2 La-Mg-Ni-Al and La-Mg-Ni-Al-D systems

All samples in the La–Mg–Ni–Al system have been analyzed exclusively by PXD. Summary of the performed phase analysis is presented in Table 3 and 4, Figure 3 and supplementary materials. The collected diffraction patterns confirm a multiphase nature of all synthesized compositions. The calculated unit cell parameters for corresponding phases vary among samples with different Al concentration, signifying uneven distribution of the substituting elements (Mg, Al) in the formed structures. Only two of the studied powders, B_{AM}-$Al_{0.1}$, prepared by arc melting, and B_{IMPC}-$Al_{0.2}$, synthesized by induction melting, contain the targeted A_2B_7-type structure. Its abundance equals 79 wt.% and 1 wt.%, in B_{AM}-$Al_{0.1}$ and B_{IMPC}-$Al_{0.2}$, respectively. While the latter one additionally consists of four other phases, in the former one only 2:7*R* (8 wt.%) and $LaNi_5$ (13 wt.%) are present. Analysis of the PXD data obtained for the mechanically processed $B_{AM/BM}$-$Al_{0.07}$ confirms presence of at least four compounds: 5:19*H* (77 wt.%), 5:19*R* (14 wt.%), 1:3*R* (2 wt.%) and 1:5*H* (7 wt.%). Interestingly, in contrary to the corresponding Al-free composition synthesized in the same way ($A_{AM/BM}$), it does not form any A_2B_7-type structure. In the $B_{AM/IM}$-$Al_{0.2}$ sample series, where an influence of different synthesis methods and form of raw elements on the sample phase composition are examined, significant difference among powders are observed. While PXD data of B_{IMPC}-$Al_{0.2}$ suggest presence of 2:7*H* (1 wt.%), 5:19*H* (6 wt.%), 5:19*R* (39 wt.%), AB_3 (1 wt.%, hereafter referred to as 1:3*R*) and AB_5 (53 wt.%), the peaks in the diffraction pattern of B_{IMP}-$Al_{0.2}$ can be assigned to only three phases, 5:19*H* (1 wt.%), 1:3*R* (19 wt.%) and 1:5*H* (80 wt.%). The PXD data of the last sample in the series, B_{AM}-$Al_{0.2}$, can be successfully indexed by mixture of four crystalline compunds: 5:19*H* (33 wt.%), 5:19*R* (10 wt.%), 1:3*R* (9 wt.%) and 1:5*H* (48 wt.%). Observed compositional differences among nominally identical samples, which were prepared by different synthesis methods, suggest

high sensitivity of the superlattice structures towards the applied synthesis conditions and/or form of raw elements used during the sample fabrication.

Table 3. Unit cell parameters and phase abundance as obtained from the analysis of PXD data for samples in the La-Mg-Ni-Al system.

sample	phase & space group	*a* [Å]	*c* [Å]	*V* [Å^3]	phase abundance [wt.%]
$B_{AM/BM}$-$Al_{0.07}$	5:19*H* (*$P6_3/mmc$*)	5.0231(2)	32.129(1)	702.06(4)	77(3)
	5:19*R* (*R-3m*)	5.0319(1)	48.835(1)	1070.85(5)	14(1)
	1:3*R* (*R-3m*)	5.068(9)	25.25(8)	561(2)	1.2(3)
	1:5*H* (*P6/mmm*)	5.0165(2)	3.9613(4)	86.33(1)	7.8(5)
B_{AM}-$Al_{0.1}$	2:7*H* (*$P6_3/mmc$*)	5.0563(3)	24.402(1)	540.28(5)	79(2)
	2:7*R* (*R-3m*)	5.0570(7)	36.109(7)	799.7(2)	8(1)
	1:5*H* (*P6/mmm*)	5.0443(6)	4.0220(7)	88.63(2)	13(1)
$B_{AM/IM}$-$Al_{0.2}$/series					
B_{IMPC}-$Al_{0.2}$	2:7*H* (*$P6_3/mmc$*)	5.0581(5)	24.263(6)	537.6(2)	1.0(1)
	5:19*H* (*$P6_3/mmc$*)	5.0349(5)	32.099(2)	704.7(1)	6.0(8)
	5:19*R* (*R-3m*)	5.0460(1)	48.931(3)	1079.0(1)	39(1)
	1:3*R* (*R-3m*)	5.0804(4)	25.668(6)	573.7(1)	1.0(2)
	1:5*H* (*P6/mmm*)	5.0377(2)	4.0143(4)	88.227(8)	53(1)
B_{IMP}-$Al_{0.2}$	5:19*H* (*$P6_3/mmc$*)	5.0300(3)	31.951(5)	700.1(1)	1.0(3)
	1:3*R* (*R-3m*)	5.0746(5)	24.604(7)	548.7(1)	19(1)
	1:5*H* (*P6/mmm*)	5.0408(5)	4.0163(1)	88.380(4)	80(1)
B_{AM}-$Al_{0.2}$	5:19*H* (*$P6_3/mmc$*)	5.0301(3)	32.015(3)	701.53(9)	33(4)
	5:19*R* (*R-3m*)	5.0455(1)	48.860(2)	1077.17(6)	10.3(6)
	1:3*R* (*R-3m*)	5.0922(9)	25.094(3)	563.5(1)	9.2(6)
	1:5*H* (*P6/mmm*)	5.0446(1)	4.0222(1)	88.645(4)	47.5(7)
B_{AM}-$Al_{0.25}$	5:19*H* (*$P6_3/mmc$*)	5.0336(6)	32.027(5)	702.8(2)	14.3(8)
	1:3*R* (*R-3m*)	5.0998(3)	25.086(3)	565.04(8)	12.0(4)
	1:5*H* (*P6/mmm*)	5.04747(6)	4.03246(7)	88.971(2)	73.7(9)

Regardless of the applied synthesis route, formation of 1:5*H* is clearly favored in all samples of the $B_{AM/IM}$-$Al_{0.2}$ series and suggests high stability of the phase for the studied Al concentration. The analysis of PXD data collected for the most Al-rich sample among studied compositions (B_{AM}-$Al_{0.25}$) indicates coexistence of 5:19*H* (14 wt.%), AB_3- and AB_5-type structures (12 and 74 wt.%, respectively). The sample phase composition is identical to B_{IMP}-$Al_{0.2}$, which contains a slightly lower fraction of Al ($La_{0.774}Mg_{0.258}Ni_{3.018}Al_{0.25}$ (B_{AM}-$Al_{0.25}$) vs. $La_{0.774}Mg_{0.258}Ni_{3.068}Al_{0.2}$ (B_{IMP}-$Al_{0.2}$). The higher Al content in B_{AM}-$Al_{0.25}$ is reflected in the ~~increase of~~ enlarged lattice constants for all corresponding phases.

Besides $B_{AM/BM}$-$Al_{0.07}$, in all studied powders the calculated unit cell volume of AB_5 phase increases as compared to the data reported for the binary $LaNi_5$ (V = 87.36 Å^3, JCPDS 50-0777) and indicates a possible partial replacement of Ni by Al atoms. Comparative analysis of structural parameters for the remaining phases is however difficult at this stage since in all identified superlattice structures (2:7*H*, 2:7*R*, 5:19*H*, 5:19*R* and 1:3*R*) possible simultaneous substitution of La and Ni by Mg and Al, respectively, can take place.

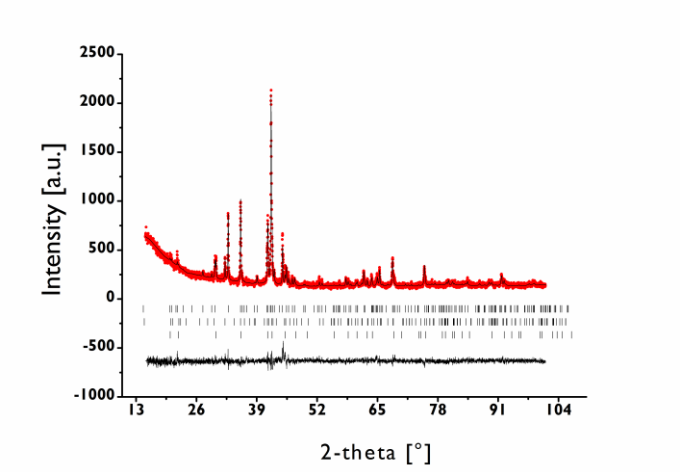

Figure 3. Observed (red), calculated (black) and difference (bottom) PXD patterns (λ = 1.54056 Å) obtained for the **B_{AM}-$Al_{0.1}$** sample. Vertical bars indicate the Bragg peak positions of contributing phases (from top to bottom 2:7*H*, 2:7*R* and 1:5*H*), χ^2 = 1.48.

The analysis of the PXD diffraction data alone does not allow to discern both processes due to the strong correlation among fitted parameters and/or values of occupancy factors for Mg and/or Al within estimated standard deviations. Additional powder diffraction data sets (e.g. PND data) or samples with limited number of superstructure phases appear to be necessary to confirm whether observed variations in unit cell volumes are related to a single atom type substitution or rather simultaneous Al and Mg incorporation into the crystal structure.

Among all investigated Al-based compositions B_{AM}-$Al_{0.1}$ is the only with a high abundance of 2:7*H* (79 wt.%) (Table 3). The powder was obtained in the same way as already reported single phase sample of $La_{0.82}Mg_{0.18}Ni_{3.5}$ [30], what provides a good basis for a consistent comparison of structural parameters between both stoichiometries. Rietveld refinement results for B_{AM}-$Al_{0.1}$ confirm that the A_2B_7-type structure reveals close similarity to the $La_{0.82}Mg_{0.18}Ni_{3.5}$ phase [30]. It retains the hexagonal symmetry of the ternary La–Mg–Ni-based parent compound but with an expanded unit cell volume. This is attributed to a purely geometrical effect resulting from differences in atomic radius among constituting elements (r_{La} = 1.87 Å vs. r_{Mg} = 1.60 Å and r_{Ni} = 1.25 Å vs. r_{Al} = 1.43 Å) and suggests possible atomic substitution(s). The structural analysis of 2:7*H* (Figure 3, Table 4) shows that Mg partially replaces La atoms, in the same way as in $La_{0.82}Mg_{0.18}Ni_{3.5}$ [30]. The substitution takes place exclusively in the $LaNi_2$ slabs and affects only one of two available *4f* sites. In the studied phase, Mg atoms occupy statistically 47 % of available sites. This is higher Mg concentration than in $La_{0.82}Mg_{0.18}Ni_{3.5}$ [30] (occupancy *n* = 37 %) and similar to the value reported for $La_{0.75}Mg_{0.25}Ni_{3.5}$ [37] (occupancy *n* = 48 %). It is however significantly smaller than in $La_{0.75}Mg_{0.25}Ni_{3.5}$ [38] (occupancy *n* = 59 %). The refined fraction of Mg in the structure should result in a reduced unit cell volume as compared to $La_{0.82}Mg_{0.18}Ni_{3.5}$ [30] and similar to the value reported for $La_{0.75}Mg_{0.25}Ni_{3.5}$ [37] . Instead, the studied A_2B_7 crystal

structure reveals opposite trend (a = 5.0563(3) Å, c = 24.402(1) Å, V = 540.28(5) Å^3 vs. a = 5.04731(8) Å, c = 24.318694) Å, V = 536.52(2) Å^3 for $La_{0.82}Mg_{0.18}Ni_{3.5}$ [30] and a = 5.0285(2) Å, c = 24.222(2) Å, V = 530.42(4) Å^3 for $La_{0.75}Mg_{0.25}Ni_{3.5}$ [37]). The observed increase of the lattice constants clearly demonstrates partial replacement of Ni by larger Al atoms. All available Ni atomic positions were checked for a possible Al substitution but the reduced fractional atomic occupancy was observed only at one of two available *6h* sites. Consequently, during the final refinement cycles the occupancy of this site was divided between Ni and Al atoms and constrained to 100%. The obtained results show that Al atoms enter exclusively $LaNi_5$ slabs and occupy statistically 12 % of the *6h* site. The refined composition of the hexagonal phase accounts for $La_{0.77(2)}Mg_{0.23(-)}Ni_{3.41(1)}Al_{0.09(-)}$ and corresponds well with the sample nominal composition ($La_{0.774}Mg_{0.258}Ni_{3.168}Al_{0.1}$). The secondary 2:7*R* phase (8 wt.%) was refined against a crystal structure model originally reported by Zhang et al. for $La_{0.75}Mg_{0.25}Ni_{3.5}$ [38]. The studied rhombohedral phase (a = 5.0570(7) Å, c = 36.109(7) Å, V = 799.7(2) Å^3) also reveals partial substitution of La by Mg atoms, which are distributed over one of two available *6c* sites (occupancy 26 %). This is in contrary to the data reported for $La_{0.75}Mg_{0.25}Ni_{3.5}$ [38], where La and Mg shared both *6c* sites (Mg occupancy: 16 % and 47 %), but similar to recently reported results for $La_{0.76}Mg_{0.24}Ni_{3.5}$ [39], where only one of two La atomic positions showed presence of Mg atoms. The concentration of Mg in 2:7*R* is much lower than in $La_{0.75}Mg_{0.25}Ni_{3.5}$ or $La_{0.76}Mg_{0.24}Ni_{3.5}$. This phase was also checked for possible Al for Ni substitution but the Rietveld refinement results did not suggest any presence of Al in the structure. Thus, the final refined phase composition is $La_{0.89(1)}Mg_{0.11(-)}Ni_{3.5(-)}$. In B_{AM}-$Al_{0.1}$, the AB_5 phase reveals the most pronounced expansion of a unit cell volume as compared with other samples studied in this paper (Table 4). The calculated lattice parameters (a = 5.0443(6) Å, c = 4.0220(7) Å, V = 88.63(2) Å^3) are bigger than reported for purely binary La–Ni intermetallic, crystallizing with the same structure

type. However, the performed structural analysis results in a full occupancy of *2c* and *3g* sites exclusively by Ni atoms and do not indicate any Al lattice incorporation. Obtained results show that Al atoms reveal a strong preference and tend to enter to the hexagonal A_2B_7-type structure rather than 2:7*R* or $LaNi_5$ in the La–Mg–Ni–Al system.

Table 4. Structural parameters of phases present in the **B_{AM}-$Al_{0.1}$** sample as obtained by Rietveld refinements of PXD data (χ^2 = 1.48, R_p = 6.61, R_{wp} = 8.50).

phase	atom	site	B_{iso} [Å^2]	*x*	*y*	*z*	occupancy
2:7*H* (79 ± 2 wt.%)							
Ce_2Ni_7-type							
	La	*4f*$_1$	0.2(2)	1/3	2/3	0.1707(4)	1.0(-)
	La	*4f*$_2$	2.2(1)	1/3	2/3	0.0247(4)	0.53(2)
	Mg	*4f*$_2$	2.2 (-)	1/3	2/3	0.0247(4)	0.47(-)
	Ni	*2a*	0.6(1)	0	0	0	1.0(-)
	Ni	*4e*	0.6(-)	0	0	0.1706(9)	1.0(-)
	Ni	*4f*$_3$	0.6(-)	1/3	2/3	0.8330(7)	1.0(-)
	Ni	*6h*	0.6(-)	0.849(4)	0.692(8)	1/4	0.88(1)
	Al	*6h*	0.6(-)	0.849(4)	0.692(8)	1/4	0.12(1)
	Ni	*12k*	0.6(-)	0.833(2)	0.665(4)	0.0836(3)	1.0(-)
$La_{0.77}Mg_{0.23}Ni_{3.41}Al_{0.09}$	**2:7*H* (*P6$_3$/mmc*), *a* = 5.0563(3), *c* = 24.402(1) Å, *V* = 540.28(5) Å^3**						
2:7*R* (8 ± 1 wt.%)							
Gd_2Co_7-type	La	*6c*$_1$		1/3	2/3	0.050(1)	1.0(-)
	La	*6c*$_2$		1/3	2/3	0.1599(9)	0.78(2)
	Mg	*6c*$_2$		1/3	2/3	0.1599(9)	0.22(-)
	Ni	*3b*		0	0	1/2	1.0(-)
	Ni	*6c*$_3$		0	0	0.274(2)	1.0(-)
	Ni	*6c*$_4$		1/3	2/3	0.372(2)	1.0(-)
	Ni	*9e*		1/2	0	0	1.0(-)
	Ni	*18h*		0.490(5)	0.510(5)	0.111(10	1.0(-)
$La_{0.89}Mg_{0.11}Ni_{3.5}$	**2:7*R* (*R-3m*), *a* = 5.0570(7), *c* = 36.109(7) Å, *V* = 799.7(2) Å^3, $B_{iso\_overall}$ = 3.4(6) Å^2**						
1:5*H* (13 ± 1 wt.%)							
$CaCu_5$-type							
	La	*1a*		0	0	0	1
	Ni	*2c*		1/3	2/3	0	1
	Ni	*3g*		1/2	0	1/2	1
$LaNi_5$	**1:5*H* (*P6/mmm*), *a* = 5.0443(6), *c* = 4.0220(7) Å, *V* = 88.63(2) Å^3, $B_{iso\_overall}$ = 2.2(3) Å^2**						

The hexagonal A_2B_7-type structure in the B_{AM}-$Al_{0.1}$, the powder was studied further and deuterated *ex situ* in a stainless steel autoclave, at room temperature and under 10 bar of D_2 gas. The analysis of the collected PXD data indicates the D-induced lattice expansion of all present phases, without any symmetry change (Figure 4, Table 5). While the increase of a unit cell volume is almost identical for both A_2B_7 polymorphs ($\Delta V/V$ = 23.5 % and 22.6 %, for 2:7*H* and 2:7*R*, respectively), for $LaNi_5$ it reaches 19.3 %. The observed expansion of the hexagonal cell (2:7*H*) is smaller than for Al-free $La_{0.82}Mg_{0.18}Ni_{3.5}$ [30] and $La_{0.75}Mg_{0.25}Ni_{3.5}$ [37] ($\Delta V/V$ = 25.6 % and 25.2 %, respectively). The lattice constants change isotropically ($\Delta a/a$ = 6.5 %, $\Delta c/c$ = 8.9 %) similar to the ternary compositions ($\Delta a/a$ = 7.3 %, $\Delta c/c$ = 9.1 % for $La_{0.82}Mg_{0.18}Ni_{3.5}$ and $\Delta a/a$ = 7.1 %, $\Delta c/c$ = 9.1 % for $La_{0.75}Mg_{0.25}Ni_{3.5}$). The obtained values are smaller than for $La_{0.82}Mg_{0.18}Ni_{3.5}$ [30] and $La_{0.75}Mg_{0.25}Ni_{3.5}$ [37], which crystallized as a single hexagonal A_2B_7-type structure. However, they are bigger from numbers reported for other 2:7*H* phases in the La–Mg–Ni system (e. g. $\Delta a/a$ = 6.03 %, $\Delta c/c$ = 7.59 % in [47]; $\Delta a/a$ = 7.03 %, $\Delta c/c$ = 6.9 % in [41]), which were investigated as part of the multiphase samples.

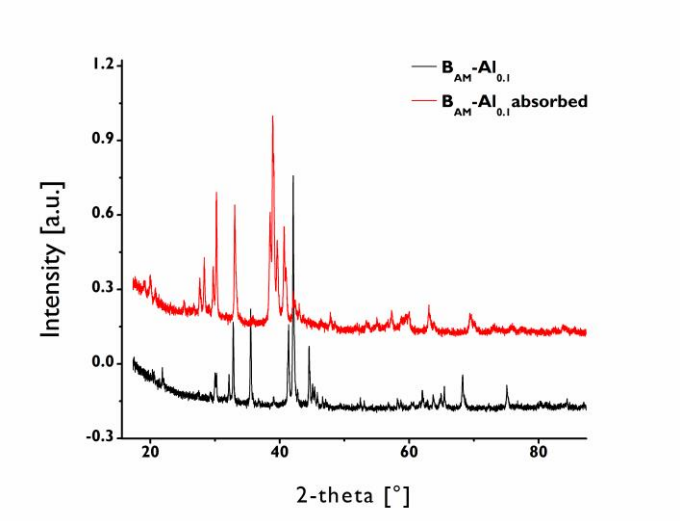

Figure 4. PXD patterns (λ = 1.54056 Å) collected for the **B_{AM}-$Al_{0.1}$** sample before (black) and after (red) D_2 absorption.

The unit cell expansion of the rhombohedral structure is 6.6 % and 7.9 %, in the basal *ab* plane and *c* direction, respectively. Both are in a good agreement with previously reported values for the corresponding rhombohedral A_2B_7 phases (e.g. $\Delta a/a$ = 7.4 %, $\Delta c/c$ = 5.9 % in [46] ; $\Delta a/a$ = 6.9 %, $\Delta c/c$ = 9.0 % in [41]; $\Delta a/a$ = 6.05 %, $\Delta c/c$ = 7.58 % in [47]).

Table 5. Unit cell parameters obtained from the analysis of PXD data for the deuterated **B_{AM}-$Al_{0.1}$**. The amount of absorbed deuterium (per formula unit (f.u.) and per metal atom (M)) was calculated from the volumetric difference using Peisl's relationship [35].

sample	phase & space group	*a* [Å]	*c* [Å]	*V* [Å^3]	$\Delta a/a$ [%]	$\Delta c/c$ [%]	$\Delta V/V$ [%]	D/f.u.	D/M
B_{AM}-$Al_{0.1}$	2:7*H* (*P6$_3$/mmc*)	5.3851(6)	26.573(3)	667.4(1)	6.5	8.9	23.5	8.1	0.9
	2:7*R* (*R-3m*)	5.3911(6)	38.965(7)	980.7(2)	6.6	7.9	22.6	7.8	0.9
	1:5*H* (*P6/mmm*)	5.3612(7)	4.2472(8)	105.7(1)	6.3	5.5	19.3	6.7	1.1

Further studies of both Al-based intermetallic compounds and their hydrides/deuterides, should be pursed in order to describe the detailed D-atom distributions within metal atom substructures. Since it is very unlikely to reduce a number of phases in the La–Mg–Ni–Al system, it would be wise to explore an idea about the probable range of structural changes related to a substitution by a single atom type only. Thus, independent studies on exclusively Al-substituted superlattice structures in the binary La–Mg system are needed.

4. Conclusions

The presented observations confirm the formation of A_2B_7-type structure in mechanically processed samples of the La–Mg–Ni system. The obtained powders reveals a multiphase nature as compared to the nominally identical samples prepared by the conventional metallurgical approach. The hexagonal Al-substituted $(La,Mg)_2(Ni, Al)_7$ phase can be

successfully synthesized by arc melting. In the investigated crystal structure of $La_{0.77}Mg_{0.23}Ni_{3.41}Al_{0.09}$, the Al atoms occupy 12 % of the *6h* site within the $LaNi_5$ slabs. This intermetallic absorbs hydrogen/deuterium when exposed to 10 bar of H_2/D_2 gas at room temperature. The H/D-containing phase expands isotropically and retains the original symmetry of the parent compound. The observed results suggest the important role of the applied synthesis methodology on the formation of superlattice compounds in both ternary La–Ni–Mg and quaternary La–Mg–Ni–Al systems. Analysis of the collected PXD and PND data underlines the advantage of neutron diffraction studies in the examination of systems containing closely related crystal structure, for which PXD experiments do not provide unambiguous results.

References

[1] Young KH, Nei J. The current status of hydrogen storage alloy development for electrochemical applications. Materials. 2013;6:4574-608.
[2] Yartys V, Noreus D, Latroche M. Metal hydrides as negative electrode materials for Ni-MH batteries. Appl Phys a-Mater. 2016;122:1-11.
[3] Buschow KHJ, Vanmal HH. Phase relations and hydrogen absorption in lanthanum-nickel system. J Less-Common Met. 1972;29:203-10.
[4] Liu YF, Cao YH, Huang L, Gao MX, Pan HG. Rare earth-Mg-Ni-based hydrogen storage alloys as negative electrode materials for Ni/MH batteries. J Alloy Compd. 2011;509:675-86.
[5] Yasuoka S, Magari Y, Murata T, Tanaka T, Ishida J, Nakamura H, et al. Development of high-capacity nickel-metal hydride batteries using superlattice hydrogen-absorbing alloys. J Power Sources. 2006;156:662-6.
[6] Kohno T, Yoshida H, Kawashima F, Inaba T, Sakai I, Yamamoto M, et al. Hydrogen storage properties of new ternary system alloys: La_2MgNi_9, $La_5Mg_2Ni_{23}$, La_3MgNi_{14}. J Alloy Compd. 2000;311:L5-L7.
[7] Ozaki T, Kanemoto M, Kakeya T, Kitano Y, Kuzuhara M, Watada M, et al. Stacking structures and electrode performances of rare earth-Mg-Ni-based alloys for advanced nickel-metal hydride battery. J Alloy Compd. 2007;446:620-4.
[8] Gal L, Charbonnier V, Zhang JX, Goubault L, Bernard P, Latroche M. Optimization of the La substitution by Mg in the La_2Ni_7 hydride-forming system for use as negative electrode in Ni-MH battery. Int J Hydrogen Energ. 2015;40:17017-20.
[9] Zhang L, Han SM, Han D, Li Y, Zhao X, Liu JJ. Phase decomposition and electrochemical properties of single phase La1.6Mg0.4Ni7 alloy. J Power Sources. 2014;268:575-83.
[10] Liu YF, Pan HG, Gao MX, Wang QD. Advanced hydrogen storage alloys for Ni/MH rechargeable batteries. J Mater Chem. 2011;21:4743-55.
[11] Wu Z, Kishida K, Inui H, Ishida J, Yasuoka S, Zhang Z. Microstructures and hydrogen absorption–desorption behavior of an A_2B_7-based La-Mg-Ni alloy. Int J Hydrogen Energ. 2017;42:22159-66.
[12] Feng F, Geng M, Northwood DO. Electrochemical behaviour of intermetallic-based metal hydrides used in Ni/metal hydride (MH) batteries: a review. Int J Hydrogen Energ. 2001;26:725-34.
[13] Nishimura K, Takasaki T, Sakai T. Introduction of large-sized nickel-metal hydride battery GIGACELL for industrial applications. J Alloy Compd. 2013;580:S353-S8.
[14] Pollet BG, Staffell I, Shang JL. Current status of hybrid, battery and fuel cell electric vehicles: From electrochemistry to market prospects. Electrochim Acta. 2012;84:235-49.
[15] Cao ZJ, Ouyang LZ, Wang H, Liu JW, Sun DL, Zhang QA, et al. Structural characteristics and hydrogen storage properties of Sm_2Co_7. J Alloy Compd. 2014;608:14-8.
[16] Ouyang LZ, Cao ZJ, Li LL, Wang H, Liu JW, Min D, et al. Enhanced high-rate discharge properties of $La_{11.3}Mg_{6.0}Sm_{7.4}Ni_{61.0}Co_{7.2}Al_{7.1}$ with added graphene synthesized by plasma milling. Int J Hydrogen Energ. 2014;39:12765-72.
[17] Cao ZJ, Ouyang LZ, Li LL, Lu YS, Wang H, Liu JW, et al. Enhanced discharge capacity and cycling properties in high-samarium, praseodymium/neodymium-free, and low-cobalt A_2B_7 electrode materials for nickel-metal hydride battery. Int J Hydrogen Energ. 2015;40:451-5.
[18] Liu JJ, Han SM, Li Y, Zhang JL, Zhao YM, Che LD. Effect of crystal transformation on electrochemical characteristics of La-Mg-Ni-based alloys with A_2B_7-type super-stacking structures. Int J Hydrogen Energ. 2013;38:14903-11.
[19] Zhao Y, Gao MX, Liu YF, Huang L, Pan HG. The correlative effects of Al and Co on the structure and electrochemical properties of a La-Mg-Ni-based hydrogen storage electrode alloy. J Alloy Compd. 2010;496:454-61.
[20] Liu JJ, Han SM, Li Y, Yang SQ, Zhang L, Zhao YM. Effect of Al incorporation on the degradation in discharge capacity and electrochemical kinetics of La-Mg-Ni-based alloys with $A_{(2)}B_{(7)}$-type super-stacking structure. J Alloy Compd. 2015;619:778-87.

[21] Young K, Ouchi T, Wang L, Wong DF. The effects of Al substitution on the phase abundance, structure and electrochemical performance of $La_{0.7}Mg_{0.3}Ni_{2.8}Co_{0.5-x}Al_x$ (x=0, 0.1, 0.2) alloys. J Power Sources. 2015;279:172-9.
[22] Tian X, Wei W, Duan RX, Zheng XY, Zhang HW, Tegus O, et al. Preparation and electrochemical properties of $La_{0.70}Mg_xNi_{2.45}Co_{0.75}Al_{0.30}$ (x=0, 0.30, 0.33, 0.36, 0.39) hydrogen storage alloys. J Alloy Compd. 2016;672:104-9.
[23] Dong XP, Yang LY, Li XT, Wang Q, Ma LH, Lin YF. Effect of substitution of aluminum for nickel on electrochemical properties of $La_{0.75}Mg_{0.25}Ni_{3.5-x}Co_{0.2}Al_x$ hydrogen storage alloys. J Rare Earth. 2011;29:143-9.
[24] Jiang WQ, Mo XH, Guo J, Wei YY. Effect of annealing on the structure and electrochemical properties of $La_{1.8}Ti_{0.2}MgNi_{8.9}Al_{0.1}$ hydrogen storage alloy. J Power Sources. 2013;221:84-9.
[25] Li RF, Xu PZ, Zhao YM, Wan J, Liu XF, Yu RH. The microstructures and electrochemical performances of $La_{0.6}Gd_{0.2}Mg_{0.2}Ni_{3.0}Co_{0.5-x}Al_x$ (x=0-0.5) hydrogen storage alloys as negative electrodes for nickel/metal hydride secondary batteries. J Power Sources. 2014;270:21-7.
[26] Zhang L, Han SM, Li Y, Liu JJ, Zhang JL, Wang JD, et al. Formation mechanism, phase structure and electrochemical properties of the La-Mg-Ni-based multiphase alloys by powder sintering $LaNi_5$ and $LaMgNi_4$. Int J Hydrogen Energ. 2013;38:10431-7.
[27] Yartys VA, Vajeeston P, Riabov AB, Ravindran P, Denys RV, Maehlen JP, et al. Crystal chemistry and metal-hydrogen bonding in anisotropic and interstitial hydrides of intermetallics of rare earth (R) and transition metals (T), RT_3 and R_2T_7. Z Kristallogr. 2008;223:674-89.
[28] Iwase K, Mori K. Crystal structure and hydrogen storage property of Nd_2Ni_7 superlattice alloy. Int J Hydrogen Energ. 2013;38:5316-21.
[29] Iwase K, Mori K, Hoshikawa A, Ishigaki T. Hydrogenation and structural properties of Gd_2Ni_7 with superlattice structure. Int J Hydrogen Energ. 2012;37:5122-7.
[30] Guzik MN, Hauback BC, Yvon K. Hydrogen atom distribution and hydrogen induced site depopulation for the $La_{2-x}Mg_xNi_7$-H system. J Solid State Chem. 2012;186:9-16.
[31] Li YM, Zhang YH, Ren HP, Liu ZC, Sun H. Mechanism of distinct high rate dischargeability of La_4MgNi_{19} electrode alloys prepared by casting and rapid quenching followed by annealing treatment. Int J Hydrogen Energ. 2016;41:18571-81.
[32] Dong XP, Pang YR, Yang LY, Wang Q, Li ZY. Effect of spark plasma sintering temperature on electrochemical properties of $La_{0.82}Mg_{0.18}Ni_{3.50}Co_{0.15}$ alloy. J Iron Steel Res Int. 2016;23:459-65.
[33] Huot J, Ravnsbaek DB, Zhang J, Cuevas F, Latroche M, Jensen TR. Mechanochemical synthesis of hydrogen storage materials. Prog Mater Sci. 2013;58:30-75.
[34] Chebab S, Abdellaoui M, Latroche M, Paul-Boncour V. Structural and hydrogen storage properties of $LaCaMgNi_9$-type alloy obtained by mechanical alloying. Mater Renew Sustain Energy. 2015;4:1-10.
[35] Peisl H. Lattice strains due to hydrogen in metals. Berlin: Springer Berlin Heidelberg; 1978.
[36] Rodriguez Carvajal J. Recent advances in magnetic-structure determination by neutron powder diffraction. Physica B. 1993;192:55-69.
[37] Denys RV, Riabov AB, Yartys VA, Sato M, Delaplane RG. Mg substitution effect on the hydrogenation behaviour, thermodynamic and structural properties of the La_2Ni_7-$H(D)_{(2)}$ system. J Solid State Chem. 2008;181:812-21.
[38] Zhang FL, Luo YC, Chen JP, Yan RX, Chen JH. La-Mg-Ni ternary hydrogen storage alloys with Ce_2Ni_7-type and Gd_2Co_7-type structure as negative electrodes for Ni/MH batteries. J Alloy Compd. 2007;430:302-7.
[39] Zhang JX, Latroche M, Magen C, Serin V, Hytch MJ, Knosp B, et al. Investigation of the phase occurrence, H sorption properties, and electrochemical behavior in the composition ranges $La_{0.75-0.80}Mg_{0.30-0.38}Ni_{3.67}$. J Phys Chem C. 2014;118:27808-14.
[40] Ferey A, Cuevas F, Latroche M, Knosp B, Bernard P. Elaboration and characterization of magnesium-substituted La_5Ni_{19} hydride forming alloys as active materials for negative electrode in Ni-MH battery. Electrochim Acta. 2009;54:1710-4.

[41] Nakamura J, Iwase K, Hayakawa H, Nakamura Y, Akiba E. Structural study of La_4MgNi_{19} hydride by in situ X-ray and neutron powder diffraction. J Phys Chem C. 2009;113:5853-9.
[42] Zhang L, Zhang JL, Han SM, Li Y, Yang SQ, Liu JJ. Phase transformation and electrochemical properties of $La_{0.70}Mg_{0.30}Ni_{3.3}$ super-stacking metal hydride alloy. Intermetallics. 2015;58:65-70.
[43] Wan CB, Denys RV, Yartys VA. In situ neutron powder diffraction study of phase-structural transformations in the La-Mg-Ni battery anode alloy. J Alloy Compd. 2016;670:210-6.
[44] Liu JJ, Han SM, Li Y, Zhang L, Zhao YM, Yang SQ, et al. Phase structures and electrochemical properties of La-Mg-Ni-based hydrogen storage alloys with superlattice structure. Int J Hydrogen Energ. 2016;41:20261-75.
[45] Gao ZJ, Kang L, Luo YC. Influence of magnesium content on structure and performance of A_2B_7-type RE-Mg-Ni hydrogen storage alloys. Chem J Chinese U. 2012;33:2035-42.
[46] Zhang JX, Villeroy B, Knosp B, Bernard P, Latroche M. Structural and chemical analyses of the new ternary La_5MgNi_{24} phase synthesized by Spark Plasma Sintering and used as negative electrode material for Ni-MH batteries. Int J Hydrogen Energ. 2012;37:5225-33.
[47] Liu JJ, Han SM, Li Y, Zhang JL, Zhao YM, Che LD. Effect of crystal transformation on electrochemical characteristics of La-Mg-Ni-based alloys with $A_{(2)}B_{(7)}$-type super-stacking structures. Int J Hydrogen Energ. 2013;38:14903-11.